

Alma Mater Studiorum Università di Bologna  
Archivio istituzionale della ricerca

Five-Degree-of-Freedom Pose Estimation from an Imaged Ellipsoid of Revolution

This is the final peer-reviewed author's accepted manuscript (postprint) of the following publication:

*Published Version:*

Modenini, D. (2019). Five-Degree-of-Freedom Pose Estimation from an Imaged Ellipsoid of Revolution. JOURNAL OF SPACECRAFT AND ROCKETS, 56(3), 952-958 [10.2514/1.A34340].

*Availability:*

This version is available at: <https://hdl.handle.net/11585/670355> since: 2020-02-27

*Published:*

DOI: <http://doi.org/10.2514/1.A34340>

*Terms of use:*

Some rights reserved. The terms and conditions for the reuse of this version of the manuscript are specified in the publishing policy. For all terms of use and more information see the publisher's website.

This item was downloaded from IRIS Università di Bologna (<https://cris.unibo.it/>).  
When citing, please refer to the published version.

(Article begins on next page)

This is the final peer-reviewed accepted manuscript of:

Modenini, D. Five-degree-of-freedom pose estimation from an imaged ellipsoid of revolution (2019) Journal of Spacecraft and Rockets, 56 (3), pp. 952-958.

The final published version is available online at: <http://arc.aiaa.org/loi/jsrdoi:10.2514/1.A34340>

#### Rights / License:

The terms and conditions for the reuse of this version of the manuscript are specified in the publishing policy. For all terms of use and more information see the publisher's website.

*This item was downloaded from IRIS Università di Bologna (<https://cris.unibo.it/>)*

***When citing, please refer to the published version.***

# **Five Degrees of Freedom Pose Estimation From an Imaged Ellipsoid of Revolution**

D. Modenini,<sup>1</sup>

*Research Fellow, Department of Industrial Engineering, University of Bologna, via Fontanelle 40, 47121, Forlì,  
Italy.*

---

<sup>1</sup> Research Fellow, Department of Industrial Engineering (DIN), University of Bologna, via Fontanelle 40, 47121, Forlì, Italy.

## Nomenclature

$\mu$	=	eigenvalues ratio
$a$	=	spheroid major radius, m
$C$	=	3x3 homogeneous conic matrix
$c$	=	spheroid minor radius, m
$f$	=	focal length, m
$f_l$	=	flattening parameter
$k$	=	dimensionless range
$K$	=	matrix of intrinsic camera parameters
$Q$	=	4x4 homogeneous quadric matrix
$R$	=	attitude matrix
$T$	=	3x4 roto-translation transformation matrix
$t$	=	translation vector, m
$\mathbf{x}$	=	3-D homogeneous image plane coordinates, m
$\mathbf{x}$	=	4-D homogeneous point coordinates, m
$\alpha$	=	scaling factor
$\lambda$	=	eigenvalue
$\mathbf{v}$	=	line-of-sight unit vector
$\rho$	=	range, $m$
$\tau$	=	longitude
$\varphi$	=	latitude
$V, W$	=	orthogonal matrices
$D$	=	diagonal matrix

### *Subscripts*

n	=	NED frame
w	=	world frame
c	=	camera frame

### *Superscripts*

\* = adjoint

$T$  = transpose

## **I.Introduction**

The capability of autonomously determine its own position may reduce dramatically the operational costs of a spacecraft (SC). One technique which can be profitably exploited in this sense is the optical navigation (OPNAV), which seeks to determine the relative position between the spacecraft and an imaged celestial body.

Especially in the recent years, several authors tackled the problem of finding analytical solutions to the OPNAV problem when the imaged target is an ellipsoid, provided that the attitude with respect to an ellipsoid fixed frame is known [1-6]. The attitude with respect to an inertial frame is usually available onboard of a SC through one, or more, star trackers. Then, if the inertial orientation of the ellipsoid is known (e.g. by specifying the spin axis and rotation rate), the attitude of the SC with respect to the ellipsoid can be computed.

In this note we address the problem of the relative pose determination (i.e. relative attitude and position) from an imaged ellipsoid of revolution. Apart from the general interest from a theoretical viewpoint, this topic is of practical application both for interplanetary OPNAV and for attitude determination, as many spacecraft are equipped with horizon sensors detecting the limb of an ellipsoid-like body, the Earth.

We will show that, exploiting some analytical results available for the perspective projection of quadrics, the pose estimation problem can be solved analytically for an ellipsoid of revolution (i.e. a spheroid) for five degrees of freedom (DOF), thus computing the entire camera pose apart from the only DOF which is unobservable due to symmetry, viz the longitude of observation. Moreover, for the 5 detectable DOF two ambiguities will be shown to arise as a direct consequence of the symmetry of the ellipsoid with respect to its meridian planes, ambiguities that cannot be resolved unless other information is made available.

The results obtained can be employed for 1) coarse OPNAV information in situation of unavailable attitude information (i.e. lost-in space situation, star-tracker failure), or inaccurate knowledge of the rotational state of the target and 2) for a horizon sensor implementation, which exploits the information on the target oblateness without the need of knowing the point of observation by independent means.

This note is organized as follows: first, we recall the mathematical background of pinhole projective transformations. Secondly, we formulate the problem of pose estimation from imaged ellipsoids. Closed form expressions of the range and of the absolute value of the latitude of observation are given as a function of the eigenvalue ratios of two symmetric matrices. Then, the camera attitude is provided as the solution of a modified Orthogonal Procrustes problem, extending some earlier results from the author [7]. The performance of the algorithm is tested by applying the algorithm both on synthetically generated images and actual images of Ceres gathered by Dawn spacecraft. Finally, the sensitivity of the accuracy to variations in illumination conditions is addressed through a set of Monte Carlo-like simulations.

## II. Mathematical Formulation

We adopt a standard projective camera model for which the homogeneous 4-D coordinates of a point in world frame,  $\mathbf{x}_w = [x \ y \ z \ 1]^T$ , maps to the image plane according to the transformation [8]:

$$\mathbf{x} = KR[I \ \mathbf{t}_w]\mathbf{x}_w \quad (1)$$

In Eq. (1)  $R$  is the attitude (rotation) matrix mapping from the world frame to camera (body) frame;  $\mathbf{t}_w$  is the translation vector from the camera center to the origin of the coordinate system, expressed in world coordinates;  $K$  is the intrinsic camera matrix: for an ideal pinhole camera having optical axis aligned with  $z$ , and the  $x$ - $y$  plane parallel

to the image sensor array, the intrinsic camera matrix is  $K = \begin{bmatrix} f & 0 & 0 \\ 0 & f & 0 \\ 0 & 0 & 1 \end{bmatrix}$ ,  $f$  being the focal length;  $\mathbf{x} = [fx \ fy \ z]^T$  is

the vector of homogeneous image plane coordinates. Therefore, Eq. (1) relates the four-dimensional homogeneous coordinates of a point in space expressed in the world frame, to its three-dimensional homogeneous projection on the image plane expressed in camera frame, by combining the roto-translation between the two frames to the projective transformation  $K$ .

Without loss of generality, we consider an ellipsoid centered in the origin of the world frame, with axes aligned to those of the world frame,  $z$  being the symmetry axis. The points on its surface are described through the homogeneous quadric equation:

$$\mathbf{x}_w^T Q \mathbf{x}_w = 0 \quad (2)$$

where:

$$Q = \begin{bmatrix} 1/a^2 & 0 & 0 & 0 \\ 0 & 1/a^2 & 0 & 0 \\ 0 & 0 & 1/c^2 & 0 \\ 0 & 0 & 0 & -1 \end{bmatrix} \quad (3)$$

and  $a$  and  $c$  are the semi-axes length. All the subsequent analysis will rely on the following known result from perspective geometry [8]: under the transformation  $T = R[I \quad \mathbf{t}_w]$ , the quadric  $Q$  transforms to a conic  $C$  (i.e. a 3x3 symmetric matrix) on the image plane, according to:

$$C^* \propto K T Q^* T^T K^T \quad (4)$$

where  $*$  superscript stands for adjoint quadric (conic), which in case of an ellipsoid (ellipse) equates to the inverse, thus  $Q^* = Q^{-1}$  ( $C^* = C^{-1}$ ). The inverse quadric (conic) is the locus of the planes (lines) tangent to the original quadric (conic). The geometric interpretation of Eq. (4) is the following: when imaging an ellipsoid, we retrieve an ellipse on the image plane as the intersection of the cone tangent to the ellipsoid, and whose vertex is lying on the camera center, with the plane itself.

Eq. (4) is valid up to a scale factor, since the symmetric matrix  $C$  represents a conic in homogeneous coordinates which, in turn, is fully determined by 5 independent parameters. Therefore, the 3x3 matrix representation of a conic is invariant to a scale factor. If we define  $\mathcal{C}^* = K^{-1} C^* K^{-T}$ , we may rewrite Eq. (4) as:

$$\alpha \mathcal{C}^* = T Q^* T^T \quad (5)$$

with  $\alpha$  being an unknown constant.  $\mathcal{C}$  and  $\mathcal{C}^*$  are computed starting from the coefficients of the ellipse quadratic equation:

$$Ax^2 + Bxy + Cy^2 + Dx + Ey + G = 0 \quad (6)$$

In particular, for an ideal pinhole camera having intrinsic matrix  $K = \begin{bmatrix} f & 0 & 0 \\ 0 & f & 0 \\ 0 & 0 & 1 \end{bmatrix}$ , it follows:

$$\mathcal{C} = \begin{bmatrix} Af^2 & \frac{Bf^2}{2} & \frac{Df}{2} \\ \frac{Bf^2}{2} & Cf^2 & \frac{Ef}{2} \\ \frac{Df}{2} & \frac{Ef}{2} & G \end{bmatrix} \quad (7)$$

and:

$$\mathcal{C}^* = \begin{bmatrix} \frac{E^2 - 4CG}{f^2\kappa} & \frac{2BG - DE}{f^2\kappa} & \frac{2CD - BE}{f\kappa} \\ \frac{2BG - DE}{f^2\kappa} & \frac{D^2 - 4AG}{f^2\kappa} & \frac{2AE - BD}{f\kappa} \\ \frac{2CD - BE}{f\kappa} & \frac{2AE - BD}{f\kappa} & \frac{B^2 - 4AC}{\kappa} \end{bmatrix} \quad (8)$$

$$\kappa = GB^2 - BDE + CD^2 + AE^2 - 4ACG$$

Since the inverse quadric matrix  $Q^*$  admits the block-diagonal decomposition  $Q^* = \begin{bmatrix} Q_3^* & \mathbf{0} \\ \mathbf{0} & -1 \end{bmatrix}$ , the rotational and translational part of the transformation in Eq. (5) can be decoupled, according to:

$$\alpha\mathcal{C}^* = R(Q_3^* - \mathbf{t}_w\mathbf{t}_w^T)R^T = R(Q_3^* - \rho^2\mathbf{v}_w\mathbf{v}_w^T)R^T \quad (9)$$

where we used the notation  $Q_3^* = Q^*(1:3,1:3)$  and  $\mathbf{t}_w = \rho\mathbf{v}_w$ ,  $\rho$  being the range and  $\mathbf{v}_w$  the line-of-sight unit vector from the camera to the spheroid center, function of latitude  $\varphi$  and longitude  $\tau$ :

$$\mathbf{v}_w = -[\cos(\varphi)\cos(\tau) \quad \cos(\varphi)\sin(\tau) \quad \sin(\varphi)]^T \quad (10)$$

In many practical applications, such as for orbiting spacecraft or for instrument target pointing, it is more convenient to consider the camera attitude with respect to a frame related the local vertical, rather than an ellipsoid fixed frame. One frame which is commonly employed is the NED (North-East-Down) one. We can formulate the pose estimation problem to solve for the attitude with respect to such a frame. First, we write the attitude matrix  $R$  as the combination of two rotations:

$$R = R_{c/n}R_{n/w} \quad (11)$$

where  $R_{n/w}$  is the rotation matrix from the world frame to NED frame, and  $R_{c/n}$  is the rotation matrix from NED to camera frame, in general function of longitude and latitude. Upon substitution of Eq. (11), Eq. (9) can be rewritten as:

$$\alpha\mathcal{C}^* = R_{c/n}R_{n/w}(Q_3^* - \mathbf{t}_w\mathbf{t}_w^T)R_{n/w}^TR_{c/n}^T = R_{c/n}(Q_n^* - \mathbf{t}_n\mathbf{t}_n^T)R_{c/n}^T = R_{c/n}\left(Q_n^* - \begin{bmatrix} 0 & 0 & 0 \\ 0 & 0 & 0 \\ 0 & 0 & \rho^2 \end{bmatrix}\right)R_{c/n}^T \quad (12)$$

where  $Q_n^* = R_{n/w}Q_3^*R_{n/w}^T$ ,  $\mathbf{t}_n = R_{n/w}\mathbf{t}_w = [0 \ 0 \ \rho]^T$ ,  $\rho$  being the range from the camera to the ellipsoid center. Then, defining

$$B_n^* = Q_n^* - \begin{bmatrix} 0 & 0 & 0 \\ 0 & 0 & 0 \\ 0 & 0 & \rho^2 \end{bmatrix} \quad (13)$$

Eq. (12) is rewritten as:



$$B_n^* = \alpha R_{c/n}^T \mathcal{C}^* R_{c/n} \quad (14)$$

Eq. (14) states that  $B_n^*$  and  $\alpha \mathcal{C}^*$  are orthogonally similar matrices. The pose estimation problem can be conveniently split in two stages, viz a first one, consisting of computing the point of observation such that  $B_n^*$  and  $\alpha \mathcal{C}^*$  are similar; and a second stage, which solves for the orthogonal matrix  $R_{c/n}$ . Since matrix  $B_n^*$  is a symmetric 3x3 matrix, it owns real eigenvalues which can be computed in closed form using Cardano's formula. In particular, it holds:

$$\begin{aligned} \lambda_1 &= a^2 \\ \lambda_{2,3} &= \frac{a^2 + c^2 - \rho^2 \pm \sqrt{(a^2 - c^2)(a^2 - c^2 - 2\rho^2 \cos 2\varphi) + \rho^4}}{2} \end{aligned} \quad (15)$$

Note that  $\lambda_1$  and  $\lambda_2$  are positive, while  $\lambda_3$  is negative (provided that the point of observation is outside of the spheroid surface). Furthermore, the eigenvalues are independent from the longitude of observation, as one may expect due to the assumed symmetry of revolution. That is, only 5 DOF can be determined, namely  $(\rho, \varphi)$  and three independent parameters of matrix  $R_{c/n}$ . This mathematical result reflects what can be intuitively inferred when thinking of a camera nadir pointing towards a spheroid: by keeping the range and latitude fixed, and allowing the longitude to vary while shooting images, all images would look exactly the same, which makes the longitude unobservable. It is easy to verify that, for  $\varphi = 90^\circ$  Eqs. (15) simplify to:

$$\begin{aligned} \lambda_1 &= a^2 \\ \lambda_2 &= a^2 \\ \lambda_3 &= c^2 - \rho^2 \end{aligned} \quad (16)$$

That is, two eigenvalues are coincident, and equal to the equatorial radius. While for  $\varphi = 0^\circ$  it holds:

$$\begin{aligned} \lambda_1 &= a^2 \\ \lambda_2 &= c^2 \\ \lambda_3 &= a^2 - \rho^2 \end{aligned} \quad (17)$$

Since  $B_n^*$  and  $\alpha \mathcal{C}^*$  are orthogonally similar, they have the same eigenvalues. However, when we image an ellipsoid,  $\mathcal{C}^*$  only is known ( $\alpha$  being undetermined), thus we may better state that  $B_n^*$  and  $\mathcal{C}^*$  have the same eigenvalue ratios. We can then write a system of two equations in the unknowns  $\rho, \varphi$  requiring that:

$$\begin{aligned}
\frac{\lambda_1}{\lambda_3} &= \frac{2a^2}{a^2 + c^2 - \rho^2 - \sqrt{(a^2 - c^2)(a^2 - c^2 - 2\rho^2 \cos 2\varphi) + \rho^4}} \\
&= \frac{2}{1 + f_l^2 - k^2 - \sqrt{(1 - f_l^2)(1 - f_l^2 - 2k^2 \cos 2\varphi) + k^4}} \\
\frac{\lambda_3}{\lambda_2} &= \frac{a^2 + c^2 - \rho^2 - \sqrt{(a^2 - c^2)(a^2 - c^2 - 2\rho^2 \cos 2\varphi) + \rho^4}}{a^2 + c^2 - \rho^2 + \sqrt{(a^2 - c^2)(a^2 - c^2 - 2\rho^2 \cos 2\varphi) + \rho^4}} \\
&= \frac{1 + f_l^2 - k^2 - \sqrt{(1 - f_l^2)(1 - f_l^2 - 2k^2 \cos 2\varphi) + k^4}}{1 + f_l^2 - k^2 + \sqrt{(1 - f_l^2)(1 - f_l^2 - 2k^2 \cos 2\varphi) + k^4}}
\end{aligned} \tag{18}$$

are equal to the corresponding eigenvalue ratios of matrix  $\mathcal{C}^*$ , which we call  $\mu_i, i = 1, 2, 3$ . In Eq. (18), two dimensionless parameters are introduced,  $f_l = c/a$  and  $k = \rho/a$ , the first being related to the flattening of the ellipsoid, the other to the range of observation. It is easy to verify that for  $f_l = 1$  (i.e. a perfect sphere) the ratios in Eq. (18) simplifies to:

$$\begin{aligned}
\frac{\lambda_1}{\lambda_3} &= \frac{1}{1 - k^2} \\
\frac{\lambda_3}{\lambda_2} &= 1 - k^2
\end{aligned} \tag{19}$$

and clearly only the range can be retrieved. One may thus expect that, the closer the flattening parameter is to one, the lower the detectability of the latitude will be. This is also apparent when looking at the intervals that the ratios in Eq. (18) spans when letting the latitude to vary between  $0^\circ$  and  $90^\circ$ :

$$\begin{aligned}
\frac{\lambda_1}{\lambda_3} &\in \left[ \frac{1}{1 - k^2}, \frac{1}{f_l^2 - k^2} \right], \text{ for } \varphi \in [0, \pi/2] \\
\frac{\lambda_3}{\lambda_2} &\in \left[ \frac{1 - k^2}{f_l^2}, f_l^2 - k^2 \right], \text{ for } \varphi \in [0, \pi/2]
\end{aligned} \tag{20}$$

which tend to Eq. (19) as  $f_l$  approaches 1. The system of two equations is of second degree in  $k^2$ ,  $\cos 2\varphi$  and can be solved analytically, leading to:

$$\begin{aligned}
k^2 &= 1 + f_l^2 - \frac{1 + \mu_2}{\mu_1 \mu_2} \\
\cos 2\varphi &= \frac{\mu_1 - 2 + \mu_1 \mu_2 - \mu_1^2 \mu_2 + f_l^2 \mu_1 (1 + \mu_2) - f_l^4 \mu_1^2 \mu_2}{\mu_1 (1 - f_l^2) [1 + \mu_2 - (1 + f_l^2) \mu_1 \mu_2]}
\end{aligned} \tag{21}$$

Eq. (21) provides the sought for solution for the range and latitude of observation to the given spheroid, without prior knowledge of the attitude. Actually, the second of Eq. (21) leaves the sign of  $\varphi$  undetermined. This is a

consequence of the fact that the spheroid is symmetric with respect to the  $z = 0$  plane. Once  $\varphi$  and  $\rho$  are known, matrix  $B_n^*$  can be computed using Eq. (13), with  $R_{n/w}$  set equal to:

$$R_{n/w} = \begin{bmatrix} -\sin\varphi & 0 & \cos\varphi \\ 0 & 1 & 0 \\ -\cos\varphi & 0 & -\sin\varphi \end{bmatrix} \quad (22)$$

The problem of attitude determination can now be solved as a modified orthogonal Procrustes problem [7]. To solve for the attitude matrix, we make use of the spectral theorem for symmetric matrices to write:

$$\alpha \mathcal{C}^* = V D_C V^T; B_n^* = W D_B W^T \quad (23)$$

with  $V, W$  orthogonal matrices. Now, it is easy to verify that by setting

$$R_{c/n} = V W^T \quad (24)$$

Eq. (14) is satisfied, provided that the eigenvalues are arranged in the same order relative to each other. Actually, any matrix of the form:

$$R_{c/n} = V P W^T \quad (25)$$

with  $P = \text{diag}\{\pm 1 \pm 1 \pm 1\}$  will be a solution, too. The above holds, however, only in an ideal case. Indeed, because of measurement errors,  $D_C$  will differ from  $D_B$ ; nevertheless, we can still employ Eq. (24) as an estimator for  $R_{c/n}$ . In [7] it was proved that Eq. (25) provides an optimal estimate of  $R_{c/n}$  in a least squares sense, as it solves the following modified orthogonal Procrustes problem:

$$\min_R \|AR - RB\|_F^2 \quad \text{subject to } R^T R = I \quad (26)$$

Of the eight possible solutions given by Eq. (25), only four will have determinant equal to +1, thus being proper rotation matrices. Of these four, only two corresponds to the camera pointing towards the ellipsoid. Then, there will be a two-fold ambiguity left in the solution that cannot be resolved, which is a direct consequence of the symmetry of the spheroid surface with respect to its meridian planes. To select the correct solution some additional independent information is needed, e.g. past attitude history or angular information obtained from other sensors.

Finally, it is worth noting that since the eigenvectors of  $\mathcal{C}^*$  are independent from matrix scaling, there is no need of computing  $\alpha$  for getting the attitude solution.

### A. Summary of the algorithm

The 5-DOF pose estimation from an imaged ellipsoid of revolution can be summarized in the following steps:

1. Detect the limb from the gathered image.

2. Fit an ellipse to the detected limb pixels' coordinates.
3. Compute matrix  $\mathcal{C}^*$  from the ellipse coefficients according to Eq. (8).
4. Compute the range and latitude of observation according to Eq. (21).
5. Compute matrix  $B_n^*$  according to Eq. (13).
6. Compute matrices  $W$  and  $V$ , from the spectral decomposition of  $B_n^*, \mathcal{C}^*$ .
7. Choose the four  $P_i$  matrices having determinant of the same sign than the one of the product  $VW^T$ , such that  $R_i = VP_iW^T$  provides a proper rotation matrix.
8. Select the only two possible attitude solutions corresponding to the camera pointing towards the target, by checking the sign of the third component of the nadir vector expressed in camera frame.

Points 1 and 2 would deserve some extensive considerations, however, since they are not the core of this work, we will not pursue such topics in detail. For a discussion on edge detection applied to images of celestial bodies for optical navigation, the reader is referred to [4]. Many methods have been developed for fitting points to an ellipse, and usually these are divided into direct and iterative methods. As demonstrated in [1], in general the most accurate methods are the ones belonging to the iterative family, and the one used during the numerical validation of this work is of this kind [9]. In this respect, the entire process described herein cannot be strictly considered as analytical, rather from step 3 to 8 only.

### **III. Validation of the method**

#### **A. Accuracy assessment against synthetic and real images**

The proposed method is tested on a scenario assuming to image Ceres dwarf planet. Ceres is well approximated by a spheroid having equatorial and polar axes of 482.1 and 445.9 km respectively, which corresponds to a flattening parameter  $f_l = 0.925$ . To validate the method and assess its potential accuracy, we adopt a three-step approach: first, we synthetically generated images of the best fit spheroid resembling Ceres, as computed after Dawn mission. Second, we test it on a set of synthetically generated images of a polyhedron built according to publicly available Ceres shape model [10]. Finally, the algorithm is verified against a set of images of Ceres taken by the

1024×1024 Dawn primary Framing Camera (FC2)<sup>2</sup>. After Dawn, a small degree of triaxiality was observed in Ceres, with a deviation of the two equatorial radii of about 1 km with respect to the spheroid one [10]. Further, the digital elevation model developed using stereophotogrammetry reported in [12], shows a deviation of Ceres surface up to about +/- 9 km ( $\approx 2\%$  of the mean radius) with respect to the reference spheroid surface. Such a deviation is well observable in the images; thus, it is expected to cause a significant degradation of the pose determination accuracy.

Step a) is conceived to check the consistency of the method applied to an ideal condition and to assess its potential maximum accuracy both in fully and partially illuminated conditions; step b) is aimed at addressing the performance degradations to be expected due to a target shape which departs from a spheroid. Finally, step c) is devoted to the assessment of the algorithm performance under a representative deep space mission scenario. For this last step, images were retrieved from the Planetary Science Data System, which is highly acknowledged [13].

The only information needed to run the algorithm is the focal length of the camera, and the values of the two semi-axes of the target. Generated images are processed using a convolutional operator for sub-pixel limb detection, which was recently developed and tested on OPNAV images [2]. An ellipse is then fitted to the detected limb pixels using the method described in [9]. Finally, the algorithm presented in Section V is applied to each image to compute the 5 DOF pose parameters.

Note that the limb detection algorithm needs some setting parameters, which have been adjusted manually for the numerical tests. Depending on the setting, non-negligible changes in the detected limb points and in the values of the resulting pose DOF, occur. Nevertheless, the main features and trends which are reported in the following discussion remain practically unaltered.

Three scenarios are considered, corresponding to different Dawn mission phases, with the target completely or partially illuminated. The relative location and attitude between the camera and the target, the sub-solar point longitude and latitude are retrieved using spice-kernels and from the ancillary image information files and collected in Table 1. The spheroid and polyhedron synthetic images are generated using Matlab® 3D scene control tool, by replicating the same Sun-target-camera geometry of the corresponding real images. Then, for each scenario a set of

---

<sup>2</sup> FC2 field of view (FOV) is approximately 5.47 deg (IFOV =  $5.34 \times 10^{-3}$  deg); the focal length is approximately 150.1 mm [11].

100 images is created, which are obtained by convoluting the nominal synthetic image with a gaussian kernel having randomly generated standard deviation, thus adding some blur. Errors in terms of range, latitude, and NED to camera angles (defined by a ZYX rotation sequence with angles yaw, pitch and roll) are collected in Table 2, Table 3, and Table 4, for the best-fit spheroid, polyhedral model and images from Dawn, respectively. Results for the synthetic images are given in terms of root mean square error over the 100 image samples.

For the perfect spheroids (Table 2), the range relative accuracy is in the order of  $10^{-5}$  when the target occupies a large portion of the FOV (scenario 1 and 2); when the target occupies a small fraction of the FOV (scenario 3), the accuracy lowers to  $10^{-4}$ . The latitude of observation is detected with errors of tenths of a degree (1 and 2), rising up to more than one degree for scenario 3. The attitude angles are computed with accuracy down to  $10^{-4}/10^{-3}$  degrees, which translates to some tenths of the angular aperture of a pixel. For the partially illuminated scenarios, the yaw angle (about nadir) error is higher than the pitch-roll ones by about 2 orders of magnitude.

As one may expect, when switching to an imperfect spheroid (Table 3 and Table 4) the estimation accuracy reduces significantly. Indeed, range relative accuracy now spans in the range  $10^{-3}$  (large target) to  $10^{-2}$  (small target). This is deemed a satisfactory result, especially when considering the departure of Ceres surface from the reference ellipsoid (up to 2%) and the comparable results in [2], which are obtained from synthetic images of the Moon with terrain variation. Estimation accuracy for the off-nadir attitude angles is in the order of  $10^{-3}$  to  $10^{-2}$  degrees, which translates to fractions of a pixel up to few pixels. Yaw errors increase of about one order of magnitude with respect to the spheroid case, now amounting to few degrees. For image 2 the accuracy is the worst ( $\approx 14^\circ$ ); this effect is to be ascribed to a combination of the high latitude of observation plus the partial limb visibility. Indeed, as the latitude of observation increases, the observability of the yaw angle lowers down, ultimately becoming null at  $90^\circ$  due to the axial symmetry [7].

The least observable DOF is the latitude of observation. Errors in Table 3 and Table 4 range from a few up to almost twenty degrees. The dramatic increase with respect to the ideal spheroid is to be expected, according to the comments to Eqs. (19) and (20) in Section II: since celestial bodies typically feature a low degree of flattening, the sensitivity of the latitude estimate to errors in the computation of the imaged ellipse eigenvalues ratios is high.

An alternative interpretation of the observability of the various DOF can be obtained when noting that the range and the off-nadir angles (roll and pitch), together fix the position of the target in the camera frame, and that the yaw and latitude angles are linked to the relative orientation between the camera and ellipsoid frame. Therefore, our

results suggest that the target position can be accurately determined in the camera frame, while a coarser accuracy is expected for the relative orientation between the camera and the ellipsoid frames.

**Table 1: Image used for validating the pose estimation algorithm with geometric and illumination data**

#	image name	time	latitude [deg]	longitude [deg]	range [km]	solar lat. [deg]	solar long. [deg]	yaw [deg]	pitch [deg]	roll [deg]
1	FC21B0036884	2015-126	1.4827	53.3258	14086.918	3.8905	60.8440	77.2227	-0.1621	-0.5425
	15126003736F1F	00:37:36.128								
2	FC21B0036426	2015-121	67.8438	59.7088	14060.013	3.873	2.4781	-9.0755	0.7709	0.3179
	15121070003F1G	07:00:03.020								
3	FC21B0033630	2015-050	11.795	-174.541	46278.041	3.490	142.795	-1.7596	-0.0095	-0.0044
	15050162536F8G	16:25:36.558								

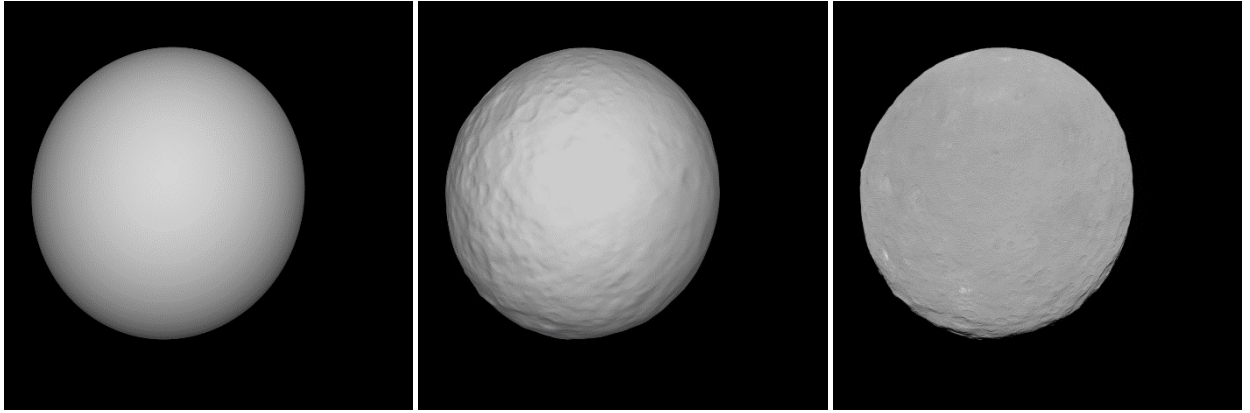


**Fig. 1 Images for scenario 1; synthetic ellipsoid (left), synthetic polyhedron (center), image from Dawn (right).**

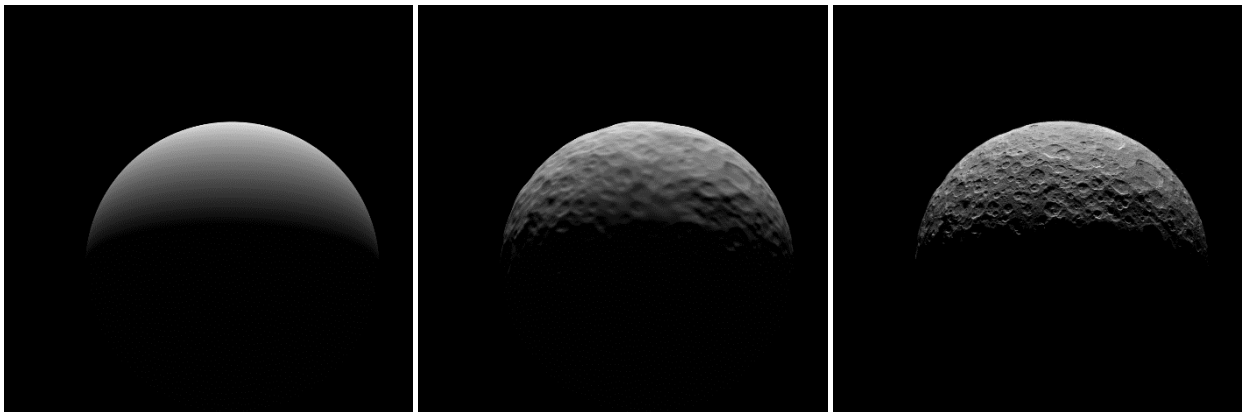


**Fig. 2 Images for scenario 2; synthetic ellipsoid (left), synthetic polyhedron (center), image from Dawn (right).**

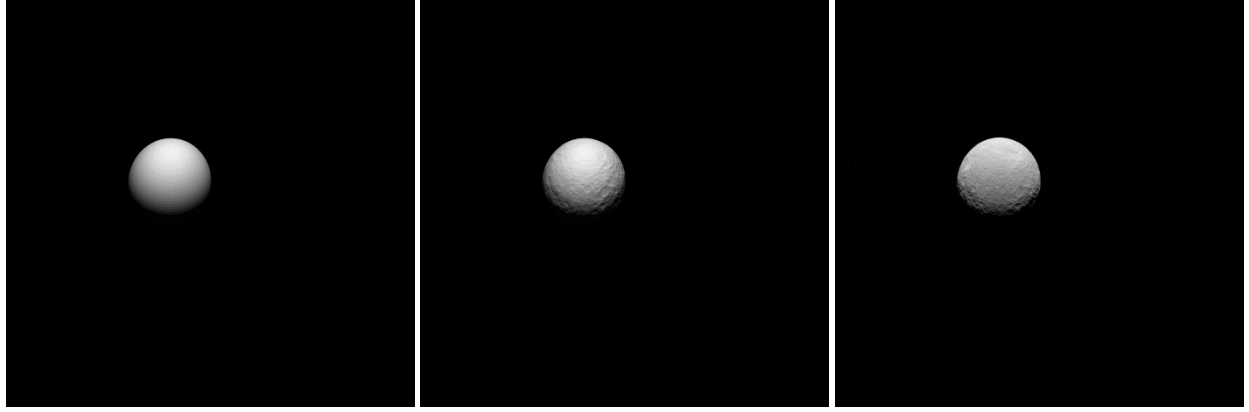


**Fig. 3** Images for scenario 3; synthetic ellipsoid (left), synthetic polyhedron (center), image from Dawn (right).

**Table 2: 5 DOF errors for synthetic images of Ceres best-fit spheroid**

Image #	range error		latitude error	yaw error		pitch error		roll error	
	[km]	[%]	[deg]	[deg]	[px]	[deg]	[px]	[deg]	[px]
1	4.179	0.030	0.283	$1.73 \times 10^{-3}$	0.33	$0.88 \times 10^{-3}$	0.17	$3.28 \times 10^{-3}$	0.61
2	0.958	0.007	0.248	0.318	59.57	$0.35 \times 10^{-3}$	0.066	$1.60 \times 10^{-3}$	0.299
3	87.938	0.190	1.125	0.187	35.06	$1.02 \times 10^{-3}$	0.19	$0.74 \times 10^{-3}$	0.14

**Table 3: 5 DOF errors for synthetic images of Ceres polyhedron shape model**

Image #	range error		latitude error	yaw error		pitch error		roll error	
	[km]	[%]	[deg]	[deg]	[px]	[deg]	[px]	[deg]	[px]
1	34.832	0.247	12.176	1.096	205.18	$2.30 \times 10^{-3}$	0.43	$2.84 \times 10^{-3}$	0.53
2	42.715	0.304	8.430	1.619	302.98	$28.1 \times 10^{-3}$	5.267	$6.00 \times 10^{-3}$	1.122
3	747.710	1.615	19.254	4.480	842.56	$9.73 \times 10^{-3}$	1.83	$5.78 \times 10^{-3}$	1.08

**Table 4: 5 DOF errors for Dawn's FC2 images of Ceres**

Image #	range error		latitude error	yaw error		pitch error		roll error	
	[km]	[%]	[deg]	[deg]	[px]	[deg]	[px]	[deg]	[px]
1	-42.083	-0.298	-15.865	1.736	324.91	$7.16 \times 10^{-3}$	1.34	$4.90 \times 10^{-3}$	0.92
2	3.476	-0.0247	5.942	-14.859	$-2.78 \times 10^3$	$24.58 \times 10^{-3}$	4.60	$0.45 \times 10^{-3}$	0.085
3	288.807	0.624	-2.340	-3.449	-646.81	$4.82 \times 10^{-3}$	0.90	$-2.99 \times 10^{-3}$	-0.56

## B. Sensitivity to varying observation points and illumination conditions

To evaluate the impact of variations in the viewpoints and illumination conditions (thus available limb arc length) on the accuracy of the retrieved DOF, a Monte Carlo-like simulation has been performed. It consists of



generating a set of synthetic images, both of the ideal spheroid and polyhedron Ceres model shape, assuming the following angles variations:

- latitude of observation, between  $-60^\circ$  and  $+60^\circ$  with  $30^\circ$  step;
- solar latitude, between  $-60^\circ$  and  $+60^\circ$  with  $30^\circ$  step;
- solar longitude, between  $-150^\circ$  and  $+150^\circ$  with  $30^\circ$  step;

All the possible combinations of the above angles have been explored, leading to a total of 275 images. For each generated image, off-nadir angles are set to  $0^\circ$  while the yaw angle is assigned randomly from a uniform distribution in the interval  $[0, 2\pi]$ ; a randomly generated blur is also added as done during the validation stage. The above is repeated for the two values of observation range corresponding to scenarios #2 and #3. Results are summarized in Table 5 and Table 6 in terms of 68% and 95% bounds of the absolute value of the 5 DOF errors.

By inspection of the tables, it appears that the main considerations drawn in the previous subsection still hold when accounting for the variability of the viewpoint and illumination conditions; the errors found for the three Ceres scenarios in III.A are of the same order of magnitude than the 68% bounds outcome of the present sensitivity analysis. The 95% bounds are about 3 to 4 times higher than the 68% ones, i.e. the errors distributions are significantly more heavy-tailed than a normal one, indicating that performance is strongly affected by the illumination conditions. This holds especially true for the yaw and latitude angles, not only when looking at the polyhedral target, but also for the ideal spheroid.

By varying illumination conditions, different limb arc lengths are made available in the image, going as low as  $60^\circ$ . In our simulations, it is found that the algorithm accuracy degrades significantly when the arc length falls below about  $100^\circ$ .

**Table 5: 5 DOF errors for sensitivity analysis using images of Ceres best-fit spheroid**

Image #	range error [%]		latitude error [deg]		yaw error [deg]		pitch error [px]		roll error [px]	
	68%	95%	68%	95%	68%	95%	68%	95%	68%	95%
1	0.083	0.234	0.504	3.878	0.415	1.499	0.593	1.508	0.623	1.599
3	0.467	0.845	2.567	8.132	2.178	6.813	0.443	0.922	0.378	0.852

**Table 6: 5 DOF *rms* errors for sensitivity analysis using images of Ceres polyhedron shape model**

Image #	range error [%]		latitude error [deg]		yaw error [deg]		pitch error [px]		roll error [px]	
	68%	95%	68%	95%	68%	95%	68%	95%	68%	95%
1	0.817	2.233	9.615	29.234	8.225	29.341	3.435	9.304	3.122	9.171
3	1.338	4.211	14.605	32.540	10.619	37.979	1.787	5.353	1.941	4.501

## IV.Conclusion

In this note we provide an analytical solution to the 5 DOF pose estimation problem from imaged ellipsoids of revolution. This problem is of interest for spacecraft attitude determination and optical navigation.

Starting from the ellipsoid image, the limb is extracted and fitted to an ellipse. By making use of some analytical results from perspective geometry, the range, and the absolute value of the latitude of observation are provided as the solution of a system of equations involving the eigenvalues of the imaged conic. Finally, the attitude matrix is computed, apart from a twofold ambiguity, by solving a modified orthogonal Procrustes problem.

The consistency of the algorithm is assessed through numerical simulations with synthetically generated images of a spheroid and both synthetic and real images of Ceres dwarf planet taken by Dawn spacecraft. Results for the spheroids indicate the very good performance of the method in retrieving the 5 pose DOF. When switching to a non-ideal scenario, i.e. when the target can be only approximated by a spheroid as for Ceres, results indicate that the range and off-nadir angles are determined very accurately, while the latitude of observation and the yaw angle are detected with low accuracy. This, in turn, results in a very good determination of the target position in camera frame, and in a worse reconstruction of the relative orientation between the camera and ellipsoid frames. An assessment of the performance under variable illumination conditions is also presented, which suggests that the two least observable DOF are also the most sensitive to such variations.

The proposed closed form solution may prove useful in several applications, for example for coarse OPNAV information when the relative attitude between the spacecraft and the target is poorly constrained or, conversely, for target pointing/relative attitude determination, when the relative position between the spacecraft and the target is not well known. Future efforts are required to refine the theory outlined, including an error covariance analysis, as well as realistic error budgets under different operational scenarios.

## V.References

- [1] Christian, J.A., "Optical Navigation Using Planet's Centroid and Apparent Diameter in Image", *Journal of Guidance, Control, and Dynamics*, Vol. 38, No. 2 (2015), pp. 192-204. <https://doi.org/10.2514/1.G000872>
- [2] Christian, J.A., "Accurate Planetary Limb Localization for Image-Based Spacecraft Navigation", *Journal of Spacecraft and Rockets*, Vol. 54, No. 3, 2017, pp.708-730. doi:10.2514/1.A33692

- [3] Lightsey, G.E. and Christian, J.A., "Onboard Image-Processing Algorithm for a Spacecraft Optical Navigation Sensor System", *Journal of Spacecraft and Rockets*, Vol. 49, No. 2 (2012), pp. 337-352. <https://doi.org/10.2514/1.A32065>
- [4] Mortari, D., de Dilectis, D., and Zanetti, R., "Position Estimation Using the Image Derivative", *Aerospace*, Vol. 2, No. 3, 2015, pp. 435-460. doi:10.3390/aerospace2030435
- [5] Mortari, D., D'Souza, C.N., and Zanetti, R., "Image Processing of Illuminated Ellipsoid", *Journal of Spacecraft and Rockets*, Vol. 53, No. 3 (2016), pp. 448-456. <https://doi.org/10.2514/1.A33342>
- [6] Modenini, D., Zannoni, M. Riccardo, L. M., and Tortora, P., "An Analytical Approach to Autonomous Optical Navigation for a CubeSat Mission to a Binary Asteroid System", *Advances in the Astronautical Sciences*, Vol. 163, pp. 139-149, 2018 (in press).
- [7] Modenini, D., "Attitude Determination from Ellipsoid Observations: A Modified Orthogonal Procrustes Problem", *Journal of Guidance Control and Dynamics*, in advance, 2018. <https://doi.org/10.2514/1.G003610>.
- [8] Hartley, R., and Zisserman, A., "Action of a projective camera on quadrics", *Multiple View Geometry in Computer Vision*, 2<sup>nd</sup> ed., Cambridge University Press, New York, 2004, pp. 201-202. <https://doi.org/10.1017/CBO9780511811685>
- [9] Szpak, Z. L., Chojnacki, W., van den Hengel, A., "Guaranteed ellipse fitting with a confidence region and an uncertainty measure for centre, axes, and orientation," *Journal of Mathematical Imaging and Vision*, Vol. 52, No. 2, 2015, pp 173–199. <http://dx.doi.org/10.1007/s10851-014-0536-x>
- [10] Ermakov, A. I., Fu, R. R., Castillo-Rogez, J. C., Raymond, C. A., Park, R. S., Preusker, F., Russell, C. T., Smith, D. E., Zuber, M. T., "Constraints on Ceres' Internal Structure and Evolution From Its Shape and Gravity Measured by the Dawn Spacecraft", *Journal of Geophysical Research*, Vol.122, No.11, 2017, pp. 2267-2293. <https://doi.org/10.1002/2017JE005302>
- [11] Schröder, S.E., Maue, T., Gutiérrez Marqués, P. et al., "In-flight calibration of the Dawn Framing Camera", *Icarus*, Vol. 226, No. 2, 2013, pp. 1304-1317. <https://doi.org/10.1016/j.icarus.2013.07.036>
- [12] Preusker, F., Scholten F., Matz, K.D., Elgner, S., Jaumann, R., Roatsch, T., Joy, S.P., Polanskey, C.A., Raymond, C.A., Russell, C.T., Dawn at Ceres - Shape model and rotational state. *Proceedings of the 47<sup>th</sup> Lunar and Planetary Science Conference*, Woodlands, TX, 2016, paper number 1954.
- [13] Nathues, A., Sierks, H., Gutierrez-Marques, P., Ripken, J., Hall, I., Buettner, I., Schaefer, M., Chistensen, U., "DAWN FC2 CALIBRATED CERES IMAGES V1.0, DAWN-A-FC2-3-RDR-CERES-IMAGES-V1.0", NASA Planetary Data System, 2016.